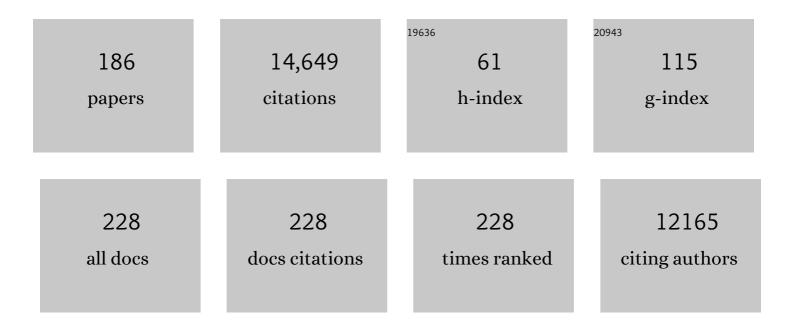
List of Publications by Year in descending order

Source: https://exaly.com/author-pdf/7710321/publications.pdf Version: 2024-02-01



#	Article	IF	CITATIONS
1	Global Estimates of Fine Particulate Matter using a Combined Geophysical-Statistical Method with Information from Satellites, Models, and Monitors. Environmental Science & Technology, 2016, 50, 3762-3772.	4.6	871
2	Advancements in the Aerosol Robotic NetworkÂ(AERONET) VersionÂ3 database – automated near-real-time quality control algorithm with improved cloud screening for Sun photometer aerosol optical depthÂ(AOD) measurements. Atmospheric Measurement Techniques, 2019, 12, 169-209.	1.2	707
3	MODIS Collection 6 MAIAC algorithm. Atmospheric Measurement Techniques, 2018, 11, 5741-5765.	1.2	505
4	Global Estimates and Long-Term Trends of Fine Particulate Matter Concentrations (1998–2018). Environmental Science & Technology, 2020, 54, 7879-7890.	4.6	431
5	Reconstructing 1-km-resolution high-quality PM2.5 data records from 2000 to 2018 in China: spatiotemporal variations and policy implications. Remote Sensing of Environment, 2021, 252, 112136.	4.6	429
6	Hyperspectral remote sensing of foliar nitrogen content. Proceedings of the National Academy of Sciences of the United States of America, 2013, 110, E185-92.	3.3	389
7	An ensemble-based model of PM2.5 concentration across the contiguous United States with high spatiotemporal resolution. Environment International, 2019, 130, 104909.	4.8	370
8	Assessing PM _{2.5} Exposures with High Spatiotemporal Resolution across the Continental United States. Environmental Science & amp; Technology, 2016, 50, 4712-4721.	4.6	360
9	Photosynthetic seasonality of global tropical forests constrained by hydroclimate. Nature Geoscience, 2015, 8, 284-289.	5.4	337
10	Improved 1 km resolution PM _{2.5} estimates across China using enhanced space–time extremely randomized trees. Atmospheric Chemistry and Physics, 2020, 20, 3273-3289.	1.9	321
11	Multiangle implementation of atmospheric correction (MAIAC): 2. Aerosol algorithm. Journal of Geophysical Research, 2011, 116, .	3.3	284
12	Estimating ground-level PM2.5 concentrations in the Southeastern United States using MAIAC AOD retrievals and a two-stage model. Remote Sensing of Environment, 2014, 140, 220-232.	4.6	274
13	A new hybrid spatio-temporal model for estimating daily multi-year PM2.5 concentrations across northeastern USA using high resolution aerosol optical depth data. Atmospheric Environment, 2014, 95, 581-590.	1.9	259
14	Vegetation dynamics and rainfall sensitivity of the Amazon. Proceedings of the National Academy of Sciences of the United States of America, 2014, 111, 16041-16046.	3.3	259
15	Estimation of daily PM10 and PM2.5 concentrations in Italy, 2013–2015, using a spatiotemporal land-use random-forest model. Environment International, 2019, 124, 170-179.	4.8	251
16	Full-coverage high-resolution daily PM2.5 estimation using MAIAC AOD in the Yangtze River Delta of China. Remote Sensing of Environment, 2017, 199, 437-446.	4.6	239
17	Spatial validation reveals poor predictive performance of large-scale ecological mapping models. Nature Communications, 2020, 11, 4540.	5.8	232
18	Multi-angle implementation of atmospheric correction for MODIS (MAIAC): 3. Atmospheric correction. Remote Sensing of Environment, 2012, 127, 385-393.	4.6	219

#	Article	IF	CITATIONS
19	Satellite observed widespread decline in Mongolian grasslands largely due to overgrazing. Global Change Biology, 2014, 20, 418-428.	4.2	218
20	Monthly Global Estimates of Fine Particulate Matter and Their Uncertainty. Environmental Science & Technology, 2021, 55, 15287-15300.	4.6	211
21	The 2010 Russian drought impact on satellite measurements of solar-induced chlorophyll fluorescence: Insights from modeling and comparisons with parameters derived from satellite reflectances. Remote Sensing of Environment, 2015, 166, 163-177.	4.6	186
22	Scientific impact of MODIS C5 calibration degradation and C6+ improvements. Atmospheric Measurement Techniques, 2014, 7, 4353-4365.	1.2	185
23	The AERONET Version 3 aerosol retrieval algorithm, associated uncertainties and comparisons to Version 2. Atmospheric Measurement Techniques, 2020, 13, 3375-3411.	1.2	176
24	Multiangle implementation of atmospheric correction (MAIAC): 1. Radiative transfer basis and look-up tables. Journal of Geophysical Research, 2011, 116, .	3.3	166
25	Using High-Resolution Satellite Aerosol Optical Depth To Estimate Daily PM _{2.5} Geographical Distribution in Mexico City. Environmental Science & Technology, 2015, 49, 8576-8584.	4.6	165
26	Multi-angle remote sensing of forest light use efficiency by observing PRI variation with canopy shadow fraction. Remote Sensing of Environment, 2008, 112, 3201-3211.	4.6	164
27	Land and cryosphere products from Suomi NPP VIIRS: Overview and status. Journal of Geophysical Research D: Atmospheres, 2013, 118, 9753-9765.	1.2	159
28	Assessing NO ₂ Concentration and Model Uncertainty with High Spatiotemporal Resolution across the Contiguous United States Using Ensemble Model Averaging. Environmental Science & Technology, 2020, 54, 1372-1384.	4.6	155
29	Predicting monthly high-resolution PM2.5 concentrations with random forest model in the North China Plain. Environmental Pollution, 2018, 242, 675-683.	3.7	146
30	Comparison and evaluation of MODIS Multi-angle Implementation of Atmospheric Correction (MAIAC) aerosol product over South Asia. Remote Sensing of Environment, 2019, 224, 12-28.	4.6	140
31	Connecting Crop Productivity, Residue Fires, and Air Quality over Northern India. Scientific Reports, 2019, 9, 16594.	1.6	133
32	Estimating daily PM 2.5 and PM 10 across the complex geo-climate region of Israel using MAIAC satellite-based AOD data. Atmospheric Environment, 2015, 122, 409-416.	1.9	130
33	Radiative transfer codes for atmospheric correction and aerosol retrieval: intercomparison study. Applied Optics, 2008, 47, 2215.	2.1	123
34	Estimation of Terrestrial Global Gross Primary Production (GPP) with Satellite Data-Driven Models and Eddy Covariance Flux Data. Remote Sensing, 2018, 10, 1346.	1.8	122
35	An automatic cloud mask algorithm based on time series of MODIS measurements. Journal of Geophysical Research, 2008, 113, .	3.3	112
36	Remote sensing of tropical ecosystems: Atmospheric correction and cloud masking matter. Remote Sensing of Environment, 2012, 127, 370-384.	4.6	112

#	Article	IF	CITATIONS
37	Earth Observations from DSCOVR EPIC Instrument. Bulletin of the American Meteorological Society, 2018, 99, 1829-1850.	1.7	108
38	Remote sensing of photosynthetic light-use efficiency across two forested biomes: Spatial scaling. Remote Sensing of Environment, 2010, 114, 2863-2874.	4.6	107
39	10-year spatial and temporal trends of PM _{2.5} concentrations in the southeastern US estimated using high-resolution satellite data. Atmospheric Chemistry and Physics, 2014, 14, 6301-6314.	1.9	106
40	Assessment of biases in MODIS surface reflectance due to Lambertian approximation. Remote Sensing of Environment, 2010, 114, 2791-2801.	4.6	103
41	Fine particulate matter predictions using high resolution Aerosol Optical Depth (AOD) retrievals. Atmospheric Environment, 2014, 89, 189-198.	1.9	100
42	Estimation of daily PM10 concentrations in Italy (2006–2012) using finely resolved satellite data, land use variables and meteorology. Environment International, 2017, 99, 234-244.	4.8	100
43	Merging regional and global aerosol optical depth records from major available satellite products. Atmospheric Chemistry and Physics, 2020, 20, 2031-2056.	1.9	98
44	Validation of highâ€resolution MAIAC aerosol product over South America. Journal of Geophysical Research D: Atmospheres, 2017, 122, 7537-7559.	1.2	97
45	Retrieval of snow grain size over Greenland from MODIS. Remote Sensing of Environment, 2009, 113, 1976-1987.	4.6	96
46	Spatial scales of pollution from variable resolution satellite imaging. Environmental Pollution, 2013, 172, 131-138.	3.7	96
47	Agricultural Burning and Air Quality over Northern India: A Synergistic Analysis using NASA's A-train Satellite Data and Ground Measurements. Aerosol and Air Quality Research, 2018, 18, 1756-1773.	0.9	95
48	Sunlight mediated seasonality in canopy structure and photosynthetic activity of Amazonian rainforests. Environmental Research Letters, 2015, 10, 064014.	2.2	90
49	Validation of GRASP algorithm product from POLDER/PARASOL data and assessment of multi-angular polarimetry potential for aerosol monitoring. Earth System Science Data, 2020, 12, 3573-3620.	3.7	90
50	Exploring systematic offsets between aerosol products from the two MODIS sensors. Atmospheric Measurement Techniques, 2018, 11, 4073-4092.	1.2	81
51	An assessment of photosynthetic light use efficiency from space: Modeling the atmospheric and directional impacts on PRI reflectance. Remote Sensing of Environment, 2009, 113, 2463-2475.	4.6	80
52	IPRT polarized radiative transfer model intercomparison project – Phase A. Journal of Quantitative Spectroscopy and Radiative Transfer, 2015, 164, 8-36.	1.1	80
53	Advances in multiangle satellite remote sensing of speciated airborne particulate matter and association with adverse health effects: from MISR to MAIA. Journal of Applied Remote Sensing, 2018, 12, 1.	0.6	79
54	Spatiotemporal prediction of fine particulate matter using high-resolution satellite images in the Southeastern US 2003–2011. Journal of Exposure Science and Environmental Epidemiology, 2016, 26, 377-384.	1.8	78

#	Article	IF	CITATIONS
55	MAIAC-based long-term spatiotemporal trends of PM2.5 in Beijing, China. Science of the Total Environment, 2018, 616-617, 1589-1598.	3.9	78
56	Tracking ambient PM2.5 build-up in Delhi national capital region during the dry season over 15 years using a high-resolution (1†km) satellite aerosol dataset. Atmospheric Environment, 2019, 204, 142-150.	1.9	78
57	Impacts of snow and cloud covers on satellite-derived PM2.5 levels. Remote Sensing of Environment, 2019, 221, 665-674.	4.6	78
58	Estimation of High-Resolution PM _{2.5} over the Indo-Gangetic Plain by Fusion of Satellite Data, Meteorology, and Land Use Variables. Environmental Science & Technology, 2020, 54, 7891-7900.	4.6	77
59	A critical assessment of high-resolution aerosol optical depth retrievals for fine particulate matter predictions. Atmospheric Chemistry and Physics, 2013, 13, 10907-10917.	1.9	71
60	Predicting Fine Particulate Matter (PM2.5) in the Greater London Area: An Ensemble Approach using Machine Learning Methods. Remote Sensing, 2020, 12, 914.	1.8	71
61	On the measurability of change in Amazon vegetation from MODIS. Remote Sensing of Environment, 2015, 166, 233-242.	4.6	67
62	Climate drivers of the Amazon forest greening. PLoS ONE, 2017, 12, e0180932.	1.1	63
63	Seasonal and interannual assessment of cloud cover and atmospheric constituents across the Amazon (2000–2015): Insights for remote sensing and climate analysis. ISPRS Journal of Photogrammetry and Remote Sensing, 2018, 145, 309-327.	4.9	60
64	Estimation of crop gross primary production (GPP): fAPARchl versus MOD15A2 FPAR. Remote Sensing of Environment, 2014, 153, 1-6.	4.6	58
65	Impacts of light use efficiency and fPAR parameterization on gross primary production modeling. Agricultural and Forest Meteorology, 2014, 189-190, 187-197.	1.9	58
66	Observations of rapid aerosol optical depth enhancements in the vicinity of polluted cumulus clouds. Atmospheric Chemistry and Physics, 2014, 14, 11633-11656.	1.9	58
67	Correcting Measurement Error in Satellite Aerosol Optical Depth with Machine Learning for Modeling PM2.5 in the Northeastern USA. Remote Sensing, 2018, 10, 803.	1.8	58
68	Airborne Spectral Measurements of Ocean Directional Reflectance. Journals of the Atmospheric Sciences, 2005, 62, 1072-1092.	0.6	55
69	Inferring terrestrial photosynthetic light use efficiency of temperate ecosystems from space. Journal of Geophysical Research, 2011, 116, .	3.3	53
70	Advancing methodologies for applying machine learning and evaluating spatiotemporal models of fine particulate matter (PM2.5) using satellite data over large regions. Atmospheric Environment, 2020, 239, 117649.	1.9	53
71	Effects of COVID-19 lockdowns on fine particulate matter concentrations. Science Advances, 2021, 7, .	4.7	53
72	Bayesian geostatistical modelling of PM10 and PM2.5 surface level concentrations in Europe using high-resolution satellite-derived products. Environment International, 2018, 121, 57-70.	4.8	51

#	Article	IF	CITATIONS
73	Analysis of a severe dust storm and its impact on air quality conditions using WRF-Chem modeling, satellite imagery, and ground observations. Air Quality, Atmosphere and Health, 2019, 12, 453-470.	1.5	50
74	Observations of the Interaction and Transport of Fine Mode Aerosols With Cloud and/or Fog in Northeast Asia From Aerosol Robotic Network and Satellite Remote Sensing. Journal of Geophysical Research D: Atmospheres, 2018, 123, 5560-5587.	1.2	49
75	Radiative transfer code SHARM for atmospheric and terrestrial applications. Applied Optics, 2005, 44, 7764.	2.1	48
76	Analysis of snow bidirectional reflectance from ARCTAS Spring-2008 Campaign. Atmospheric Chemistry and Physics, 2010, 10, 4359-4375.	1.9	48
77	Characterization of forest fire smoke event near Washington, DC in summer 2013 with multi-wavelength lidar. Atmospheric Chemistry and Physics, 2015, 15, 1647-1660.	1.9	48
78	Evaluation of the multiâ€angle implementation of atmospheric correction (MAIAC) aerosol algorithm through intercomparison with VIIRS aerosol products and AERONET. Journal of Geophysical Research D: Atmospheres, 2017, 122, 3005-3022.	1.2	48
79	A method of retrieving cloud top height and cloud geometrical thickness with oxygen A and B bands for the Deep Space Climate Observatory (DSCOVR) mission: Radiative transfer simulations. Journal of Quantitative Spectroscopy and Radiative Transfer, 2013, 122, 141-149.	1.1	47
80	Role of adjacency effect in the remote sensing of aerosol. Journal of Geophysical Research, 2001, 106, 11909-11916.	3.3	46
81	Regional atmospheric CO ₂ inversion reveals seasonal and geographic differences in Amazon net biome exchange. Global Change Biology, 2016, 22, 3427-3443.	4.2	45
82	Discrimination of biomass burning smoke and clouds in MAIAC algorithm. Atmospheric Chemistry and Physics, 2012, 12, 9679-9686.	1.9	44
83	Detecting Inter-Annual Variations in the Phenology of Evergreen Conifers Using Long-Term MODIS Vegetation Index Time Series. Remote Sensing, 2017, 9, 49.	1.8	44
84	Green's function method for the radiative transfer problem I Homogeneous non-Lambertian surface. Applied Optics, 2001, 40, 3495.	2.1	43
85	Analysis of MODIS–MISR calibration differences using surface albedo around AERONET sites and cloud reflectance. Remote Sensing of Environment, 2007, 107, 12-21.	4.6	43
86	High spatial resolution aerosol retrieval with MAIAC: Application to mountain regions. Journal of Geophysical Research, 2011, 116, n/a-n/a.	3.3	43
87	A multi-angle aerosol optical depth retrieval algorithm for geostationary satellite data over the United States. Atmospheric Chemistry and Physics, 2011, 11, 11977-11991.	1.9	40
88	AERONET Remotely Sensed Measurements and Retrievals of Biomass Burning Aerosol Optical Properties During the 2015 Indonesian Burning Season. Journal of Geophysical Research D: Atmospheres, 2019, 124, 4722-4740.	1.2	40
89	An AeroCom–AeroSat study: intercomparison of satellite AOD datasets for aerosol model evaluation. Atmospheric Chemistry and Physics, 2020, 20, 12431-12457.	1.9	40
90	Atmospheric Correction at AERONET Locations: A New Science and Validation Data Set. IEEE Transactions on Geoscience and Remote Sensing, 2009, 47, 2450-2466.	2.7	38

#	Article	IF	CITATIONS
91	Atmospheric and geometrical effects on land surface albedo. Journal of Geophysical Research, 1999, 104, 4127-4143.	3.3	37
92	Surface reflectance of Mars observed by CRISM/MRO: 1. Multiâ€angle Approach for Retrieval of Surface Reflectance from CRISM observations (MARSâ€ReCO). Journal of Geophysical Research E: Planets, 2013, 118, 514-533.	1.5	37
93	Evaluation and intercomparison of wildfire smoke forecasts from multiple modeling systems for the 2019 Williams Flats fire. Atmospheric Chemistry and Physics, 2021, 21, 14427-14469.	1.9	37
94	Improved cloud and snow screening in MAIAC aerosol retrievals using spectral and spatial analysis. Atmospheric Measurement Techniques, 2012, 5, 843-850.	1.2	36
95	SPHERICAL HARMONICS METHOD IN THE PROBLEM OF RADIATIVE TRANSFER IN THE ATMOSPHERE-SURFACE SYSTEM. Journal of Quantitative Spectroscopy and Radiative Transfer, 1999, 61, 393-404.	1.1	35
96	Estimation of crop gross primary production (GPP): I. impact of MODIS observation footprint and impact of vegetation BRDF characteristics. Agricultural and Forest Meteorology, 2014, 191, 51-63.	1.9	35
97	Validation of SOAR VIIRS Overâ€Water Aerosol Retrievals and Context Within the Global Satellite Aerosol Data Record. Journal of Geophysical Research D: Atmospheres, 2018, 123, 13,496.	1.2	34
98	Estimating daily and intra-daily PM10 and PM2.5 in Israel using a spatio-temporal hybrid modeling approach. Atmospheric Environment, 2018, 191, 142-152.	1.9	34
99	Seasonality and drought effects of Amazonian forests observed from multi-angle satellite data. Remote Sensing of Environment, 2015, 171, 278-290.	4.6	32
100	Global validation of columnar water vapor derived from EOS MODIS-MAIAC algorithm against the ground-based AERONET observations. Atmospheric Research, 2019, 225, 181-192.	1.8	32
101	Similarity of radiative transfer equation: Error analysis of phase function truncation techniques. Journal of Quantitative Spectroscopy and Radiative Transfer, 2010, 111, 1964-1979.	1.1	31
102	Estimation of crop gross primary production (GPP): II. Do scaled MODIS vegetation indices improve performance?. Agricultural and Forest Meteorology, 2015, 200, 1-8.	1.9	31
103	Estimating daily PM2.5 concentrations in New York City at the neighborhood-scale: Implications for integrating non-regulatory measurements. Science of the Total Environment, 2019, 697, 134094.	3.9	31
104	Improving satelliteâ€driven PM _{2.5} models with Moderate Resolution Imaging Spectroradiometer fire counts in the southeastern U.S Journal of Geophysical Research D: Atmospheres, 2014, 119, 11375-11386.	1.2	30
105	Seasonal monitoring and estimation of regional aerosol distribution over Po valley, northern Italy, using a high-resolution MAIAC product. Atmospheric Environment, 2016, 141, 106-121.	1.9	30
106	MAIAC Thermal Technique for Smoke Injection Height From MODIS. IEEE Geoscience and Remote Sensing Letters, 2020, 17, 730-734.	1.4	30
107	Consistency of vegetation index seasonality across the Amazon rainforest. International Journal of Applied Earth Observation and Geoinformation, 2016, 52, 42-53.	1.4	29
108	Reduction of aerosol absorption in Beijing since 2007 from MODIS and AERONET. Geophysical Research Letters, 2011, 38, n/a-n/a.	1.5	27

#	Article	IF	CITATIONS
109	Satellite-based view of the aerosol spatial and temporal variability in the Córdoba region (Argentina) using over ten years of high-resolution data. ISPRS Journal of Photogrammetry and Remote Sensing, 2018, 145, 250-267.	4.9	27
110	Amazon Forests' Response to Droughts: A Perspective from the MAIAC Product. Remote Sensing, 2016, 8, 356.	1.8	26
111	Assessing uncertainties of a geophysical approach to estimate surface fine particulate matter distributions from satellite-observed aerosol optical depth. Atmospheric Chemistry and Physics, 2019, 19, 295-313.	1.9	26
112	Green's function method in the radiative transfer problem II Spatially heterogeneous anisotropic surface. Applied Optics, 2002, 41, 5600.	2.1	24
113	Impact of environmental attributes on the uncertainty in MAIAC/MODIS AOD retrievals: A comparative analysis. Atmospheric Environment, 2021, 262, 118659.	1.9	24
114	A new method of retrieving surface bidirectional reflectance from ground measurements: Atmospheric sensitivity study. Journal of Geophysical Research, 1999, 104, 6257-6268.	3.3	23
115	An example of aerosol pattern variability over bright surface using high resolution MODIS MAIAC: The eastern and western areas of the Dead Sea and environs. Atmospheric Environment, 2017, 165, 359-369.	1.9	23
116	Three-dimensional effects in the remote sensing of surface albedo. IEEE Transactions on Geoscience and Remote Sensing, 2001, 39, 254-263.	2.7	22
117	Radiative transfer code SHARM-3D for radiance simulations over a non-Lambertian nonhomogeneous surface: intercomparison study. Applied Optics, 2002, 41, 5607.	2.1	22
118	Prototyping of LAI and FPAR Retrievals from MODIS Multi-Angle Implementation of Atmospheric Correction (MAIAC) Data. Remote Sensing, 2017, 9, 370.	1.8	21
119	Impact of aerosol layering, complex aerosol mixing, and cloud coverage on high-resolution MAIAC aerosol optical depth measurements: Fusion of lidar, AERONET, satellite, and ground-based measurements. Atmospheric Environment, 2021, 247, 118163.	1.9	21
120	Parameterized code SHARM-3D for radiative transfer over inhomogeneous surfaces. Applied Optics, 2005, 44, 7602.	2.1	20
121	Observation of mountain lee waves with MODIS NIR column water vapor. Geophysical Research Letters, 2014, 41, 710-716.	1.5	20
122	Vector radiative transfer code SORD: Performance analysis and quick start guide. Journal of Quantitative Spectroscopy and Radiative Transfer, 2017, 200, 295-310.	1.1	20
123	First Provisional Land Surface Reflectance Product from Geostationary Satellite Himawari-8 AHI. Remote Sensing, 2019, 11, 2990.	1.8	20
124	The time series technique for aerosol retrievals over land from MODIS. , 2009, , 69-99.		20
125	Local analysis of MISR surface BRF and albedo over GSFC and mongu AERONET sites. IEEE Transactions on Geoscience and Remote Sensing, 2006, 44, 1707-1718.	2.7	19
126	METHOD OF SPHERICAL HARMONICS IN THE RADIATIVE TRANSFER PROBLEM WITH NON-LAMBERTIAN SURFACE. Journal of Quantitative Spectroscopy and Radiative Transfer, 1999, 61, 545-555.	1.1	18

#	Article	IF	CITATIONS
127	AERONET-based surface reflectance validation network (ASRVN) data evaluation: Case study for railroad valley calibration site. Remote Sensing of Environment, 2011, 115, 2710-2717.	4.6	17
128	Aerosol optical depth (AOD) retrieval using simultaneous GOES-East and GOES-West reflected radiances over the western United States. Atmospheric Measurement Techniques, 2013, 6, 471-486.	1.2	17
129	High resolution aerosol data from MODIS satellite for urban air quality studies. Open Geosciences, 2014, 6, .	0.6	17
130	Assessment of urban aerosol pollution over the Moscow megacity by the MAIAC aerosol product. Atmospheric Measurement Techniques, 2020, 13, 877-891.	1.2	17
131	Gradient boosting machine learning to improve satellite-derived column water vapor measurement error. Atmospheric Measurement Techniques, 2020, 13, 4669-4681.	1.2	17
132	The Potential Impact of Satellite-Retrieved Cloud Parameters on Ground-Level PM2.5 Mass and Composition. International Journal of Environmental Research and Public Health, 2017, 14, 1244.	1.2	15
133	Photopolarimetric Sensitivity to Black Carbon Content of Wildfire Smoke: Results From the 2016 ImPACTâ€PM Field Campaign. Journal of Geophysical Research D: Atmospheres, 2018, 123, 5376-5396.	1.2	15
134	Interpolation and Profile Correction (IPC) Method for Shortwave Radiative Transfer in Spectral Intervals of Gaseous Absorption. Journals of the Atmospheric Sciences, 2003, 60, 865-871.	0.6	15
135	Vegetation chlorophyll estimates in the Amazon from multi-angle MODIS observations and canopy reflectance model. International Journal of Applied Earth Observation and Geoinformation, 2017, 58, 278-287.	1.4	14
136	Assessing snow extent data sets over North America to inform and improve trace gas retrievals from solar backscatter. Atmospheric Measurement Techniques, 2018, 11, 2983-2994.	1.2	14
137	Inferring iron-oxide species content in atmospheric mineral dust from DSCOVR EPIC observations. Atmospheric Chemistry and Physics, 2022, 22, 1395-1423.	1.9	13
138	Reply to Townsend et al.: Decoupling contributions from canopy structure and leaf optics is critical for remote sensing leaf biochemistry. Proceedings of the National Academy of Sciences of the United States of America, 2013, 110, E1075.	3.3	12
139	Matrix exponential in C/C++ version of vector radiative transfer code IPOL. Journal of Quantitative Spectroscopy and Radiative Transfer, 2019, 227, 106-110.	1.1	12
140	Revised and extended benchmark results for Rayleigh scattering of sunlight in spherical atmospheres. Journal of Quantitative Spectroscopy and Radiative Transfer, 2020, 254, 107181.	1.1	12
141	Evaluating impacts of snow, surface water, soil and vegetation on empirical vegetation and snow indices for the UtqiaÄįvik tundra ecosystem in Alaska with the LVS3 model. Remote Sensing of Environment, 2020, 240, 111677.	4.6	12
142	Retrievals of Aerosol Optical Depth and Spectral Absorption From DSCOVR EPIC. Frontiers in Remote Sensing, 2021, 2, .	1.3	12
143	Solution for atmospheric optical transfer function using spherical harmonics method. Journal of Quantitative Spectroscopy and Radiative Transfer, 2001, 68, 43-56.	1.1	11
144	A Method for Unbiased High-Resolution Aerosol Retrieval from Landsat. Journals of the Atmospheric Sciences, 2004, 61, 1233-1244.	0.6	11

#	Article	IF	CITATIONS
145	Reply to Ollinger et al.: Remote sensing of leaf nitrogen and emergent ecosystem properties. Proceedings of the National Academy of Sciences of the United States of America, 2013, 110, E2438.	3.3	11
146	Progress in Remote Sensing of Photosynthetic Activity over the Amazon Basin. Remote Sensing, 2017, 9, 48.	1.8	11
147	Seasonal Comparisons of Himawari-8 AHI and MODIS Vegetation Indices over Latitudinal Australian Grassland Sites. Remote Sensing, 2020, 12, 2494.	1.8	11
148	Aerosol Properties in Cloudy Environments from Remote Sensing Observations: A Review of the Current State of Knowledge. Bulletin of the American Meteorological Society, 2021, 102, E2177-E2197.	1.7	11
149	Monthly analysis of PM ratio characteristics and its relation to AOD. Journal of the Air and Waste Management Association, 2017, 67, 27-38.	0.9	10
150	Modifications of discrete ordinate method for computations with high scattering anisotropy: Comparative analysis. Journal of Quantitative Spectroscopy and Radiative Transfer, 2012, 113, 2040-2048.	1.1	9
151	Evaluation of Novel NASA Moderate Resolution Imaging Spectroradiometer and Visible Infrared Imaging Radiometer Suite Aerosol Products and Assessment of Smoke Height Boundary Layer Ratio During Extreme Smoke Events in the Western USA. Journal of Geophysical Research D: Atmospheres, 2021, 126, e2020ID034180.	1.2	9
152	APC: A new code for Atmospheric Polarization Computations. Journal of Quantitative Spectroscopy and Radiative Transfer, 2013, 127, 1-11.	1.1	8
153	The Relationship Between MAIAC Smoke Plume Heights and Surface PM. Geophysical Research Letters, 2020, 47, e2020GL088949.	1.5	8
154	Analysis of the radiative transfer equation with highly assymetric phase function. Journal of Quantitative Spectroscopy and Radiative Transfer, 2011, 112, 1595-1608.	1.1	7
155	MODIS solar diffuser Earthshine modeling and analysis. , 2006, 6296, 44.		6
156	Scaling estimates of vegetation structure in Amazonian tropical forests using multi-angle MODIS observations. International Journal of Applied Earth Observation and Geoinformation, 2016, 52, 580-590.	1.4	6
157	Generalization of Marshak boundary condition for non-Lambert reflection. Journal of Quantitative Spectroscopy and Radiative Transfer, 2000, 67, 457-464.	1.1	5
158	An API for Spaceborne Sub-Meter Resolution Products for Earth Science. , 2019, , .		5
159	MODIS BRDF effects over Brazilian tropical forests and savannahs: a comparative analysis. Remote Sensing Letters, 2019, 10, 95-102.	0.6	5
160	Numerical results for polarized light scattering in a spherical atmosphere. Journal of Quantitative Spectroscopy and Radiative Transfer, 2022, 287, 108194.	1.1	5
161	On the accuracy of double scattering approximation for atmospheric polarization computations. Journal of Quantitative Spectroscopy and Radiative Transfer, 2012, 113, 172-181.	1.1	4
162	Developing particle emission inventories using remote sensing (PEIRS). Journal of the Air and Waste Management Association, 2017, 67, 53-63.	0.9	4

#	Article	IF	CITATIONS
163	UV Reflectance of the Ocean from DSCOVR/EPIC: Comparisons with a Theoretical Model and Aura/OMI Observations. Journal of Atmospheric and Oceanic Technology, 2019, 36, 2087-2099.	0.5	4
164	A practical guide to writing a radiative transfer code. Computer Physics Communications, 2022, 271, 108198.	3.0	4
165	A Novel Atmospheric Correction Algorithm to Exploit the Diurnal Variability in Hypertemporal Geostationary Observations. Remote Sensing, 2022, 14, 964.	1.8	4
166	A Comparison of Multi-Angle Implementation of Atmospheric Correction and MOD09 Daily Surface Reflectance Products From MODIS. Frontiers in Remote Sensing, 2021, 2, .	1.3	4
167	Atmospheric Correction of DSCOVR EPIC: Version 2 MAIAC Algorithm. Frontiers in Remote Sensing, 2021, 2, .	1.3	3
168	A method for determining atmospheric optical parameters and surface albedo from multiangle satellite measurements: sea surface applications. IEEE Transactions on Geoscience and Remote Sensing, 1999, 37, 277-286.	2.7	2
169	Improvement of MODIS RSB calibration by minimizing the earthshine impact on solar diffuser observations. , 2006, , .		2
170	A Spatial Prescreening Technique for Earth Observation Data. IEEE Geoscience and Remote Sensing Letters, 2007, 4, 152-156.	1.4	2
171	Corrigendum to "Discrimination of biomass burning smoke and clouds in MAIAC algorithm" published in Atmos. Chem. Phys., 12, 9679–9686, 2012. Atmospheric Chemistry and Physics, 2012, 12, 10631-10631.	1.9	2
172	Analyses of high resolution aerosol data from MODIS satellite: a MAIAC retrieval, southern New England, US. Proceedings of SPIE, 2013, , .	0.8	2
173	Accuracy of RT code SORD for realistic atmospheric profiles. Proceedings of SPIE, 2016, , .	0.8	2
174	Satellite mapping of PM _{2.5} episodes in the wintertime San Joaquin Valley: a "static―model using column water vapor. Atmospheric Chemistry and Physics, 2020, 20, 4379-4397.	1.9	2
175	GeoNEX: A Geostationary Earth Observatory at NASA Earth Exchange: Earth Monitoring from Operational Geostationary Satellite Systems. , 2020, , .		2
176	Multiangle monitoring of atmospheric aerosol and surface reflectance from Mir station. IEEE Transactions on Geoscience and Remote Sensing, 1999, 37, 589-595.	2.7	1
177	Application of MAIAC high spatial resolution aerosol retrievals over Po Valley (Italy). , 2013, , .		1
178	A new code SORD for simulation of polarized light scattering in the Earth atmosphere. Proceedings of SPIE, 2016, , .	0.8	1
179	Code SHARM: fast and accurate radiative transfer over spatially variable anisotropic surfaces. , 2010, , 205-247.		1
180	Analysis of calibration difference between MODIS and MISR. , 2006, 6298, 229.		0

#	Article	IF	CITATIONS
181	Atmospheric correction of multi-angle CRISM/MRO hyperspectral data: Retrieval of aerosol optical thickness and surface reflectance. , 2011, , .		0
182	Reply to Gonsamo et al.: Effect of the Eastern Atlantic-West Russia pattern on Amazon vegetation has not been demonstrated. Proceedings of the National Academy of Sciences of the United States of America, 2015, 112, E1056-E1056.	3.3	0
183	Preliminary fAPAR <inf>chl</inf> products from MODIS and hyperion. , 2016, , .		0
184	Performance of the dot product function in radiative transfer code SORD. , 2016, , .		0
185	Surface polarized reflectance analysis for aerosol remote sensing. , 2019, , .		0
186	The AOD Sensitivity Comparison between MODIS Multi-Angle Implementation of Atmospheric Correction (MAIAC) and Standard MODIS Surface Reflectance. , 2020, , .		0